Journal of the Korean Physical Society, Vol. 74, No. 6, March 2019, pp. 614∼625

Cosmic Ray Enhancements in Lunar Radiation Environment Observed by CRaTER on the LRO

Jongdae Sohn
Korea Astronomy and Space Science Institute, Daejeon 34055, Korea

Suyeon Oh*
Department of Earth Science Education, Chonnam National University, Gwangju 61186, Korea

Yu Yi
Department of Astronomy, Space Science and Geology, Chungnam National University, Daejeon 34134, Korea

Jaejin Lee
Korea Astronomy and Space Science Institute, Daejeon 34055, Korea

(Received 11 December 2018, in final form 11 January 2019)

The Cosmic Ray Telescope for the Effects of Radiation (CRaTER) instrument onboard the Lunar Reconnaissance Orbiter (LRO) characterizes the global lunar radiation environment and its biological impacts by measuring cosmic ray (CR) radiation. By using CRaTER data, we identify the lunar CR enhancements, which are similar to the terrestrial ground level enhancements (GLEs). GLE is a sudden and short increase in CR intensity recorded by the Earth's ground neutron monitors. We examine the origins and the characteristics of CR enhancements in the lunar space environment by using the CR intensity and dose rate according to CRaTER data. In order to determine origins of CR enhancements, we also use solar proton event (SPE) data, CR data of the Advanced Composition Explorer (ACE) equipped with a Solar Isotope Spectrometer (SIS), and proton flux data of Geostationary Operational Environmental Satellite 15 (GOES15). We identified 96 CRaTER enhancements (CREs) as increases in CR events in the lunar space environment during the period June 2009-December 2017. Unlike terrestrial GLEs, CREs are much longer and more frequent. Of the 96 CREs, 43 events are associated with SPE. The values of their physical characteristics are statistically larger than those of the CREs without associated SPEs. However, such non-SPE CREs are considered to originate from solar ejections. All CREs are associated with an increase in He flux by ACE/SIS. Even though CREs are associated with a small increase in He flux, this does indicate that some materials are ejected from the Sun; rather, it indicates that all CREs are associated with solar eruptions. Because of the very weak magnetic field and extremely rare atmosphere, the lunar space environment responds to even weak solar activity. An increase in He flux observed by ACE/SIS can be useful for monitoring the eruption of energetic particles from the Sun regardless of accompanying SPEs.

PACS numbers: 95.30.Qd, 95.55.Pe, 95.85.Ry, 96.50.Ci, 96.60.Vg
Keywords: Cosmic ray, Ground level enhancements, LRO/CRaTER, ACE/SIS, Solar proton events
DOI: 10.3938/jkps.74.614

I. INTRODUCTION

The Lunar Reconnaissance Orbiter (LRO) was launched on 18 June 2009 to characterize the lunar radiation environment, identify its biological impacts, and determine any potential mitigation. The seven instruments of the LRO payload included the Cosmic Ray Telescope for the Effects of Radiation (CRaTER) [1].

The CRaTER instrument is designed to investigate the lunar and deep space radiation environments such as galactic cosmic rays (GCRs), solar energetic protons, any secondary radiation at the lunar surface, and tissue equivalent plastic (TEP) response to such radiation. These data are then used to create a radiation map overlaid on the lunar surface [2]. A micro-dosimeter mounted on the analog electronics board of the CRaTER instru-

*E-mail: suyeonoh@chonnam.ac.kr; Fax: +82-62-530-2519

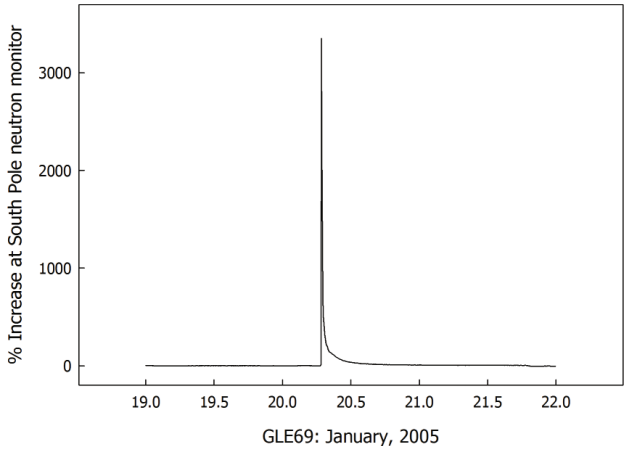

Fig. 1. Percentage increase in GLE69 that occurred on 20 January 2005, as recorded by the terrestrial South Pole neutron monitor.

ment measures dose rates below 1 μrad/s in the lunar radiation environment [3].

Neutrons as secondary particles can be detected by ground neutron monitors. Two domestic neutron monitors were installed at Daejeon in 2011 [4] and Jang Bogo station in Antarctic in 2015 [5]. Diurnal variations are typical periodic variations with sinusoid-like profiles [6]. Cosmic ray (CR) intensity depends on the modulation with solar activity in the heliosphere, and CR intensity shows the temporal decreases in variations by interplanetary magnetic structures [7–9]. The CR intensity changes suddenly owing to solar eruptions such as solar flares and coronal mass ejections. Ground level enhancement (GLE) is a representative variation in CR intensity as a response to solar activity. GLEs are rare, sudden, sharp, and short-lived increases in CR intensity measured by the Earth's ground neutron monitors [10]. The term GLE was first introduced by Forbush [11].

Figure 1 shows a GLE occurring on 20 January 2005 that was recorded at the terrestrial South Pole neutron monitor. It is the 69th and largest GLE ever recorded by the monitor, showing an increase of about 3,400%. To illustrate this increase, the figure shows GLE 69 as an example of a terrestrial GLE in a typical profile. The magnitude of GLE is expressed by the percentage increase, which is an increase in the solar cosmic ray compared with the background of GCRs.

S. Y. Oh *et al.* showed that the high energy proton flux of a solar proton event (SPE) measured by Geostationary Operational Environmental Satellite (GOES) differential channels is strongly correlated with the percentage increase of GLEs [12]. SPEs play a significant role as a source of radiation exposure for astronauts and electronic systems of spaceships. S. Y. Oh *et al.* predicted the proton flux of SPEs over various energy ranges by using the "Polar Bare Method" [13]. They also predicted the interval time between the GLE peak and peak flux of GOES proton channels. Because a GLE can be

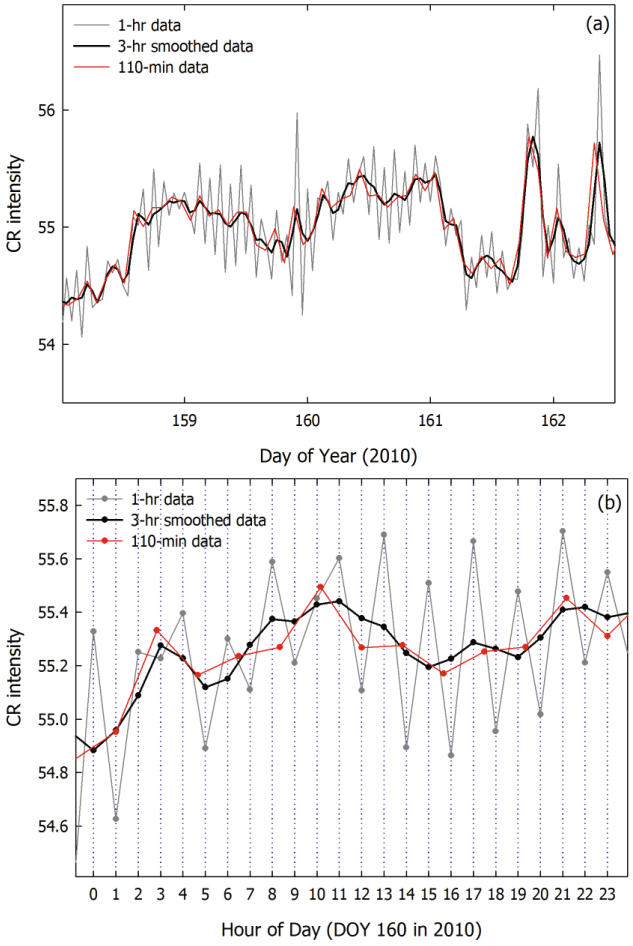

Fig. 2. (Color online) Comparison of hourly counts (thin gray line), 3 hr weighted smoothed data (thick black line), and 110 min data (red line) for (a) DOY 158-162 in 2010 and (b) DOY 160 in 2010.

detected earlier than an SPE by ground neutron monitoring, this prediction can provide information to protect against space hazards.

N. A. Schwadron *et al.* found agreement between the dose rate predicted by the model and that observed by CRaTER and showed that CRaTER can characterize the radiation environment and space weather on the Moon [14]. N. A. Schwadron *et al.* examined the dose rates in the lunar radiation environment by using prediction and observation by CRaTER [15,16]. During the declining phase of solar cycle 24, the observed dose rates exceeded the predictions, which indicate that the lunar radiation environment had worsened rapidly. This aspect of the space environment needs to be carefully considered for space missions.

Because the exact form of increases in events showing sharp profile increase in the lunar space environment is not understood this far, we examine CR enhancements in the lunar space environment in a similar method as that used for terrestrial GLE analysis. In this study, we investigated the origins and the characteristics of CRaTER

Table 1. List of 96 CREs in the lunar environment from June 2009 to December 2017.

Event	Year	Background		Onset	Maximum	Variation	CR fluence	51 hr CR fluence[3]	Duration	SPE onset (UT)	Date of	Position[4]
		Date[1]	Count[2]	(UT)	(UT)	(%)	(counts)	(counts)	(hr)	(pfu @ > 10 MeV)	lunar calendar	
C01	2010	Jun. 9, 22h	55.40	Jun. 11, 23h	Jun. 12, 4h	42.94	8.89E+06	8.89E+06	44		May.01, 2010	Out
C02	2010	Aug. 12, 8h	53.40	Aug. 14, 9h	Aug. 14, 12h	81.97	1.03E+07	1.03E+07	44	Aug. 14, 12h 30m (14)	Jul.05, 2010	Out
C03	2010	Aug. 16, 3h	54.68	Aug. 18, 4h	Aug. 18, 10h	56.62	8.65E+06	8.65E+06	38		Jul.09, 2010	Out
C04	2011	Jan. 25, 23h	52.57	Jan. 28, 0h	Jan. 28, 5h	44.19	8.89E+06	8.89E+06	39		Dec.25, 2010	Out
C05	2011	Feb. 13, 1h	53.29	Feb. 15, 2h	Feb. 15, 12h	18.44	6.83E+06	6.83E+06	32		Jan.13, 2011	In
C06	2011	Mar. 5, 18h	50.44	Mar. 7, 19h	Mar. 8, 13h	654.74	4.97E+07	3.75E+07	97	Mar. 08, 01h 05m (50)	Feb.03, 2011	Out
C07	2011	Mar. 19, 0h	50.18	Mar. 21, 1h	Mar. 21, 10h	151.93	3.00E+07	1.69E+07	119	Mar. 21, 19h 50m (14)	Feb.17, 2011	In
C08	2011	Jun. 2, 0h	47.14	Jun. 7, 5h	Jun. 7, 11h	1,972.22	8.70E+07	8.19E+07	65	Jun. 07, 08h 20m (72)	May 06, 2011	Out
C09	2011	Jul. 31, 3h	44.50	Aug. 2, 4h	Aug. 2, 10h	44.64	6.21E+06	6.21E+06	32		Jul.03, 2011	Out
C10	2011	Jul. 31, 3h	44.50	Aug. 4, 3h	Aug. 4, 9h	1,673.07	7.75E+07	7.49E+07	64	Aug. 04, 06h 35m (96)	Jul.05, 2011	Out
C11	2011	Aug. 6, 15h	46.18	Aug. 8, 16h	Aug. 8, 20h	26.86	2.55E+06	2.55E+06	13		Jul.09, 2011	Out
C12	2011	Aug. 6, 15h	46.18	Aug. 9, 5h	Aug. 9, 10h	850.06	2.28E+07	2.18E+07	57	Aug. 09, 08h 45m (26)	Jul.10, 2011	Out
C13	2011	Sep. 3, 23h	46.93	Sep. 6, 0h	Sep. 6, 9h	52.59	4.99E+06	4.99E+06	21		Aug.09, 2011	Out
C14	2011	Sep. 3, 23h	46.93	Sep. 6, 21h	Sep. 7, 4h	200.61	1.29E+07	1.29E+07	41		Aug.09, 2011	Out
C15	2011	Sep. 20, 9h	45.26	Sep. 22, 10h	Sep. 24, 1h	300.85	3.25E+07	2.22E+07	70	Sep. 23, 22h 55m (35)	Aug.25, 2011	Out
C16	2011	Sep. 20, 9h	45.26	Sep. 25, 8h	Sep. 26, 2h	394.11	2.27E+07	2.27E+07	34		Aug.28, 2011	Out
C17	2011	Oct. 20, 9h	44.57	Oct. 22, 10h	Oct. 23, 15h	43.02	1.12E+07	9.82E+06	59		Sep.26, 2011	Out
C18	2011	Nov. 1, 20h	42.93	Nov. 3, 21h	Nov. 4, 6h	87.03	2.17E+07	1.20E+07	106		Oct.08, 2011	Out
C19	2011	Nov. 24, 4h	44.42	Nov. 26, 5h	Nov. 27, 0h	790.31	3.95E+07	3.47E+07	77	Nov. 26, 11h 25m (80)	Nov.02, 2011	Out
C20	2011	Dec. 23, 15h	47.41	Dec. 25, 16h	Dec. 25, 23h	37.48	9.59E+06	9.59E+06	50		Dec.01, 2011	Out
C21	2012	Jan. 17, 0h	48.21	Jan. 23, 2h	Jan. 24, 9h	22,014.68	1.47E+09	1.36E+09	110	Jan. 23, 5h 30m (6,310)	Jan.01, 2012	Out
C22	2012	Jan. 17, 0h	48.21	Jan. 27, 16h	Jan. 28, 0h	8,629.13	4.83E+08	4.26E+08	105	Jan. 27, 19 h 05m (796)	Jan.05, 2012	Out
C23	2012	Feb. 17, 0h	44.79	Feb. 24, 22h	Feb. 25, 6h	43.41	1.01E+07	1.01E+07	48		Feb.04, 2012	Out
C24	2012	Feb. 17, 0h	44.79	Mar. 6, 23h	Mar. 7, 16h	18,948.96	1.68E+09	1.21E+09	145	Mar. 07, 5h 10m (6,530)	Feb.15, 2012	In
C25	2012	Feb. 17, 0h	44.79	Mar. 13, 15h	Mar. 13, 19h	5,023.21	1.25E+08	1.25E+08	41	Mar. 13, 18h 10m (469)	Feb.21, 2012	Out
C26	2012	May 14, 22h	44.20	May 16, 23h	May 17, 4h	3,677.66	9.89E+07	9.04E+07	90	May 17, 2h 10m (255)	Mar.27, 2012	Out
C27	2012	May 24, 18h	44.34	May 26, 19h	May 27, 10h	92.45	1.01E+07	1.01E+07	46	May 27, 5h 35m (14)	Apr.06, 2012	Out
C28	2012	Jun. 14, 11h	45.73	Jun. 16, 12h	Jun. 16, 21h	103.38	7.05E+06	7.05E+06	34	Jun. 16, 19h 55m (14)	Apr.27, 2012	Out
C29	2012	Jul. 4, 20h	41.80	Jul. 6, 21h	Jul. 7, 6h	603.35	2.02E+07	2.02E+07	43	Jul. 07, 4h 00m (25)	May 17, 2012	In
C30	2012	Jul. 4, 20h	41.80	Jul. 8, 16h	Jul. 9, 5h	528.13	2.35E+07	2.35E+07	45		May 19, 2012	Out
C31	2012	Jul. 4, 20h	41.80	Jul. 12, 13h	Jul. 12, 21h	988.26	3.43E+07	3.03E+07	66	Jul. 12, 18h 35m (96)	May 23, 2012	Out
C32	2012	Jul. 4, 20h	41.80	Jul. 17, 14h	Jul. 18, 6h	1,617.38	4.54E+07	4.54E+07	39	Jul. 17, 17h 15m (136)	May 28, 2012	Out
C33	2012	Jul. 4, 20h	41.80	Jul. 19, 5h	Jul. 19, 13h	1,892.71	8.13E+07	7.32E+07	94	Jul. 17, 17h 15m (136)	Jun.01, 2012	Out
C34	2012	Jul. 4, 20h	41.80	Jul. 23, 3h	Jul. 23, 21h	821.13	1.13E+08	5.26E+07	183	Jul. 23, 15h 45m (12)	Jun.05, 2012	Out
C35	2012	Sep. 25, 21h	43.47	Sep. 27, 22h	Sep. 28, 3h	455.15	2.05E+07	1.74E+07	69	Sep. 28, 3h 00m (28)	Aug.13, 2012	In
C36	2012	Nov. 6, 10h	39.17	Nov. 8, 11h	Nov. 8, 23h	44.67	1.89E+07	9.62E+06	112		Sep.25, 2012	Out
C37	2012	Nov. 18, 9h	39.10	Nov. 20, 10h	Nov. 20, 15h	9.25	2.74E+06	2.74E+06	18		Oct.07, 2012	Out
C38	2012	Dec. 12, 20h	38.97	Dec. 14, 21h	Dec. 15, 1h	18.53	3.10E+06	3.10E+06	20		Nov.03, 2012	Out
C39	2013	Mar. 1, 0h	41.21	Mar. 16, 1h	Mar. 16, 23h	194.12	1.18E+07	1.18E+07	43	Mar. 16, 19h 40m (16)	Feb.05, 2013	Out
C40	2013	Apr. 9, 4h	40.25	Apr. 11, 5h	Apr. 11, 15h	3,099.81	8.38E+07	7.28E+07	106	Apr. 11, 10h 55m (114)	Mar.02, 2013	Out
C41	2013	Apr. 19, 5h	39.68	Apr. 21, 6h	Apr. 21, 13h	82.44	9.49E+06	9.20E+06	53		Mar.12, 2013	Out
C42	2013	Apr. 19, 5h	39.68	Apr. 24, 18h	Apr. 25, 2h	55.75	8.18E+06	8.18E+06	48		Mar.15, 2013	In
C43	2013	May 12, 6h	39.29	May 14, 7h	May 15, 15h	1,200.73	1.16E+08	4.09E+07	166	May 15, 13h 25m (41)	Apr.05, 2013	Out
C44	2013	May 12, 6h	39.29	May 22, 10h	May 23, 5h	16,556.09	4.65E+08	4.45E+08	90	May 22, 14h 20m (1,660)	Apr.13, 2013	In
C45	2013	Jun. 19, 9h	36.29	Jun. 21, 10h	Jun. 22, 10h	111.23	1.00E+07	1.00E+07	45		May 13, 2013	In
C46	2013	Jun. 19, 9h	36.29	Jun. 23, 13h	Jun. 24, 2h	148.37	1.01E+07	1.01E+07	49	Jun. 23, 20h 14m (14)	May 13, 2013	In
C47	2013	Aug. 18, 1h	36.47	Aug. 20, 2h	Aug. 21, 13h	25.37	1.02E+07	7.60E+06	70		Jul.14, 2013	In
C48	2013	Sep. 27, 20h	35.13	Sep. 29, 21h	Sep. 30, 13h	2,266.41	9.37E+07	8.60E+07	84	Sep. 30, 05h 05m (182)	Aug.25, 2013	Out
C49	2013	Oct. 18, 11h	35.93	Oct. 28, 3h	Oct. 28, 9h	227.06	2.47E+07	1.56E+07	99		Sep.24, 2013	Out
C50	2013	Nov. 1, 4h	37.81	Nov. 2, 5h	Nov. 2, 18h	120.01	1.27E+07	1.01E+07	68		Sep.29, 2013	Out
C51	2013	Nov. 4, 22h	40.65	Nov. 6, 23h	Nov. 7, 4h	48.09	3.11E+06	3.11E+06	17		Oct.05, 2013	Out
C52	2013	Nov. 17, 8h	34.63	Nov. 19, 9h	Nov. 19, 17h	88.12	6.40E+06	6.40E+06	39		Oct.17, 2013	In
C53	2013	Dec. 24, 1h	34.37	Dec. 26, 2h	Dec. 27, 2h	64.68	9.65E+06	8.31E+06	61		Nov.24, 2013	Out
C54	2013	Dec. 24, 1h	34.37	Dec. 28, 16h	Dec. 28, 23h	557.64	1.58E+07	1.50E+07	57	Dec. 28, 21h 50m (29)	Nov.26, 2013	Out
C55	2014	Jan. 4, 5h	35.30	Jan. 6, 6h	Jan. 6, 11h	2,086.39	4.53E+07	4.53E+07	35	Jan. 06, 09h 15m (42)	Dec.06, 2013	Out
C56	2014	Jan. 4, 5h	35.30	Jan. 7, 17h	Jan. 8, 8h	19,572.50	7.89E+08	7.30E+08	89	Jan. 06, 09h 15m (1,033)	Dec.07, 2013	Out
C57	2014	Jan. 19, 8h	35.14	Jan. 21, 9h	Jan. 21, 11h	10.24	3.13E+06	3.13E+06	23		Dec.21, 2013	Out
C58	2014	Feb. 18, 5h	36.35	Feb. 20, 6h	Feb. 20, 9h	293.55	7.55E+06	7.55E+06	37	Feb. 20, 08h 50m (22)	Jan.21, 2014	Out
C59	2014	Feb. 23, 0h	31.92	Feb. 25, 1h	Feb. 28, 10h	2,020.85	1.68E+08	5.15E+07	194	Feb. 25, 13h 55m (103)	Jan.26, 2014	Out
C60	2014	Mar. 27, 15h	33.09	Mar. 29, 16h	Mar. 29, 20h	104.24	7.82E+06	7.56E+06	53		Feb.29, 2014	Out
C61	2014	Apr. 16, 10h	34.94	Apr. 18, 11h	Apr. 19, 0h	1,039.53	3.95E+07	3.84E+07	58	Apr. 18, 15h 25m (58)	Mar.19, 2014	Out
C62	2014	May 5, 15h	34.50	May 7, 16h	May 7, 21h	17.49	4.64E+06	4.64E+06	34		Apr.09, 2014	Out
C63	2014	May 5, 15h	34.50	May 9, 2h	May 9, 8h	12.62	7.42E+06	7.03E+06	54		Apr.11, 2014	In
C64	2014	Jun. 10, 18h	35.82	Jun. 12, 19h	Jun. 13, 2h	9.81	6.15E+06	6.15E+06	45		Jun.16, 2014	In
C65	2014	Aug. 23, 14h	37.36	Aug. 25, 15h	Aug. 25, 22h	23.43	7.58E+06	7.58E+06	51		Aug.01, 2014	Out

[1]Start date of background period (49 hrs).
[2]Averaged counts during the background period.
[3]The length of event is 51 hr, which is the median value of the duration.
[4]Position indicates whether the point is located in or out of the Earth's magnetosphere in a lunar orbit.

Table 1. List of 96 CREs in the lunar environment from June 2009 to December 2017.

Event	Year	Background		Onset	Maximum	Variation	CR fluence	51 hr CR fluence[3]	Duration	SPE onset (UT)	Date of	Position[4]
		Date[1]	Count[2]	(UT)	(UT)	(%)	(counts)	(counts)	(hr)	(pfu @ > 10 MeV)	lunar calendar	
C66	2014	Aug. 30, 15h	38.04	Sep. 1, 16h	Sep. 3, 4h	329.57	8.54E+07	2.30E+07	215		Aug.08, 2014	Out
C67	2014	Aug. 30, 15h	38.04	Sep. 10, 18h	Sep. 11, 5h	1,472.17	3.38E+07	3.38E+07	28		Aug.17, 2014	In
C68	2014	Aug. 30, 15h	38.04	Sep. 12, 12h	Sep. 12, 15h	1,072.38	1.28E+07	1.28E+07	20	Sep. 11, 2h 40m (126)	Aug.19, 2014	Out
C69	2014	Sep. 20, 4h	40.47	Sep. 22, 5h	Sep. 22, 12h	29.24	5.69E+06	5.69E+06	34		Aug.29, 2014	Out
C70	2014	Sep. 20, 4h	40.47	Sep. 24, 21h	Sep. 25, 2h	25.00	1.98E+07	8.68E+06	123		Sep.01, 2014	Out
C71	2014	Oct. 30, 11h	37.24	Nov. 1, 12h	Nov. 2, 21h	138.90	1.38E+07	1.04E+07	74		Sep.09, 2014	Out
C72	2014	Dec. 11, 12h	37.52	Dec. 13, 13h	Dec. 14, 9h	63.51	1.01E+07	9.04E+06	58		Oct.22, 2014	Out
C73	2014	Dec. 11, 12h	37.52	Dec. 21, 8h	Dec. 21, 18h	60.52	5.68E+06	5.68E+06	30		Oct.30, 2014	Out
C74	2014	Dec. 24, 3h	37.20	Dec. 26, 4h	Dec. 26, 10h	52.25	1.24E+07	8.15E+06	82		Nov.05, 2014	Out
C75	2015	Feb. 19, 8h	37.25	Feb. 21, 9h	Feb. 21, 17h	35.45	7.97E+06	7.97E+06	51		Jan.03, 2015	Out
C76	2015	Mar. 12, 23h	34.99	Mar. 15, 0h	Mar. 15, 7h	33.52	3.58E+06	3.58E+06	23		Jan.25, 2015	Out
C77	2015	Mar. 12, 23h	34.99	Mar. 15, 23h	Mar. 16, 9h	30.16	6.16E+06	6.16E+06	45		Jan.26, 2015	Out
C78	2015	Mar. 22, 6h	32.09	Mar. 24, 7h	Mar. 24, 15h	32.78	8.06E+06	6.92E+06	60		Feb.05, 2015	Out
C79	2015	May 10, 0h	33.69	May 12, 1h	May 12, 7h	134.52	6.96E+06	6.96E+06	40		Mar.24, 2015	Out
C80	2015	Jun. 16, 0h	36.95	Jun. 18, 1h	Jun. 18, 16h	324.12	1.83E+07	1.61E+07	65	Jun. 18, 11h 35m (16)	May.03, 2015	Out
C81	2015	Jun. 16, 0h	36.95	Jun. 21, 15h	Jun. 22, 18h	4,249.94	8.52E+07	7.94E+07	72	Jun. 21, 21h 35m (1,070)	May.06, 2015	Out
C82	2015	Jun. 16, 0h	36.95	Jun. 25, 9h	Jun. 27, 2h	259.38	2.93E+07	1.72E+07	120	Jun. 26, 3h 50m (22)	May.10, 2015	In
C83	2015	Jun. 29, 12h	38.17	Jul. 1, 13h	Jul. 1, 19h	33.20	8.15E+06	7.74E+06	54		May.16, 2015	In
C84	2015	Aug. 25, 15h	38.16	Aug. 27, 16h	Aug. 27, 23h	9.60	2.29E+06	2.29E+06	15		Jul.14, 2015	In
C85	2015	Sep. 18, 15h	39.86	Sep. 20, 16h	Sep. 20, 20h	49.02	5.81E+06	5.81E+06	36		Aug.08, 2015	Out
C86	2015	Oct. 26, 23h	40.32	Oct. 29, 0h	Oct. 29, 8h	882.05	2.63E+07	2.28E+07	73	Oct. 29, 5h 50m (23)	Sep.17, 2015	In
C87	2015	Nov. 2, 11h	41.69	Nov. 4, 12h	Nov. 4, 16h	23.01	4.91E+06	4.91E+06	31		Sep.23, 2015	Out
C88	2015	Nov. 7, 13h	40.15	Nov. 9, 14h	Nov. 10, 0h	57.70	8.11E+06	8.11E+06	50		Sep.28, 2015	Out
C89	2015	Dec. 26, 10h	45.07	Dec. 28, 11h	Dec. 29, 1h	18.97	1.39E+07	9.10E+06	81		Nov.18, 2015	Out
C90	2016	[5]Dec. 30, 21h	43.27	Jan. 1, 22h	Jan. 2, 4h	195.49	9.85E+06	9.85E+06	44	Jan. 02, 4h 30m (21)	Nov.22, 2015	Out
C91	2016	Mar. 14, 4h	46.67	Mar. 16, 5h	Mar. 16, 10h	20.84	5.11E+06	5.11E+06	28		Feb.08, 2016	Out
C92	2016	May 13, 11h	50.19	May 15, 12h	May 15, 20h	11.55	4.36E+06	4.36E+06	22		Apr.09, 2016	Out
C93	2017	Jul. 12, 0h	58.85	Jul. 14, 1h	Jul. 14, 23h	160.79	1.99E+07	1.86E+07	57	Jul. 14, 9h 00m (22)	May.21, 2017	Out
C94	2017	Sep. 2, 19h	56.60	Sep. 4, 20h	Sep. 5, 20h	882.82	4.40E+07	4.40E+07	38	Sep. 05, 0h 40m (844)	Jul.14, 2017	In
C95	2017	Sep. 2, 19h	56.60	Sep. 6, 17h	Sep. 8, 0h	4,304.64	1.32E+08	1.32E+08	46	Sep. 05, 0h 40m (844)	Jul.16, 2017	In
C96	2017	Sep. 2, 19h	56.60	Sep. 10, 14h	Sep. 10, 22h	15,347.85	1.29E+09	1.07E+09	127	Sep. 10, 16h 45m (1,490)	Jul.20, 2017	Out

[1]Start date of background period (49 hrs).
[2]Averaged counts during the background period.
[3]The length of event is 51 hr, which is the median value of the duration.
[4]Position indicates whether the point is located in or out of the Earth's magnetosphere in a lunar orbit.
[5]The previous year of the event. An SPE is defined as a flux of > 10 MeV protons and greater than 10 particles $cm^{-2}sec^{-1}ster^{-1}$ (particle flux units; pfu), as defined by NOAA SESC.

enhancements (CREs), which have profiles similar to those of terrestrial GLEs. We selected CREs by using the CR intensity measured by CRaTER and the associated solar events from the SPE data of the National Oceanic and Atmospheric Administration (NOAA) Space Environment Services Center (SESC). We also compared the CR data measured by the Solar Isotope Spectrometer (SIS) onboard Advanced Composition Explorer (ACE) as well as the solar proton flux data measured by GOES. We identified CREs and investigated the relationship between CREs and SPEs in the lunar space environment.

II. DATA AND METHODS

CRaTER is composed of six silicon detectors (D1-D6) in thin/thick pairs separated by sections of TEP, which simulates soft body tissue (muscles). This instrument has been used for both ground-based and space-based experiments.

The data set of CRaTER consists of primary and secondary science parameters and housekeeping parameters. We used the counter data of Level 2 secondary science data among the CRaTER flight data of Planetary Plasma Interaction (PPI; https://pds-ppi.igpp.ucla.edu/) and CRaTER Legacy Data Products (http://crater-products.sr.unh.edu/). CRaTER produces a daily file with 1 sec resolution. Daily files report the number of "singles" (silicon detector) as well as the numbers of "good", "rejected", and "total" records observed by CRaTER during the monitoring period. We used hourly counter data by converting the 1-s resolution data from June 2009 to December 2017. Table 5 and Figs. 20 and 21 of [2] provide information on proton threshold energy (MeV) for silicon detectors at coincidences. The first pair of thin (D1) and thick (D2) silicon detectors, which is located below the deep-space (zenith) shield endcap, has 12.7 MeV of the proton threshold energy. This threshold energy represents the cutoff energy of CR intensity by CRaTER in this study. Because the single counters receive the signals from the analog electronics subsystem, the records of the count signals are asynchronous. Thus, the same count event can be detected as a different event at each single counter. However, good counts are measured by qualifying events for all count events. Rather than representing

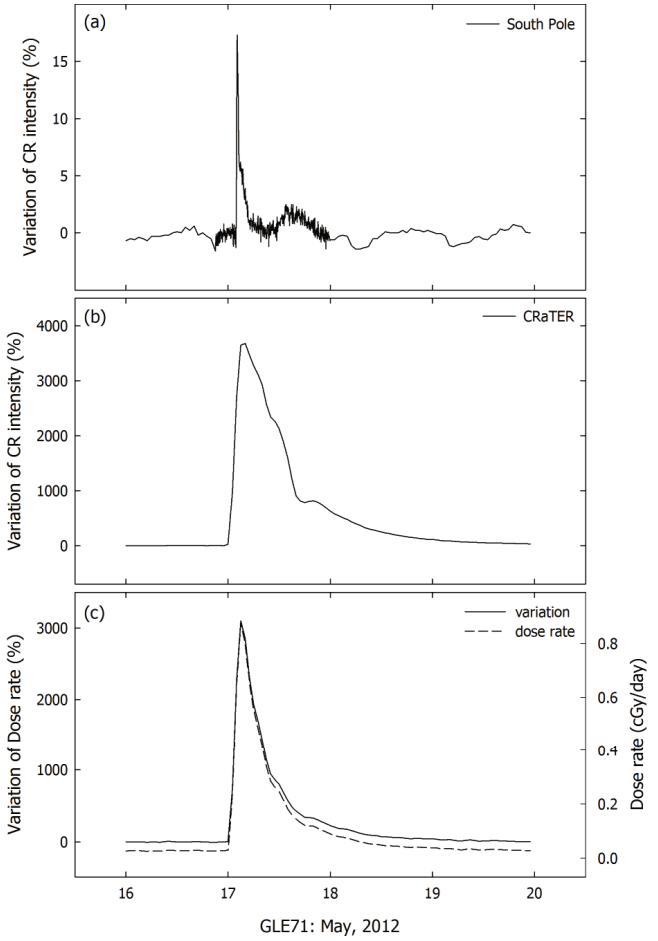

Fig. 3. Hourly profiles of CRE recorded on 17 May 2012 (C26) associated with terrestrial GLE71. From top to bottom, each panel represents the variations in CR intensity (a) at the terrestrial South Pole neutron monitor and (b) at the lunar surface by CRaTER and (c) the dose rate variation by micro-dosimeter in CRaTER in the lunar radiation environment.

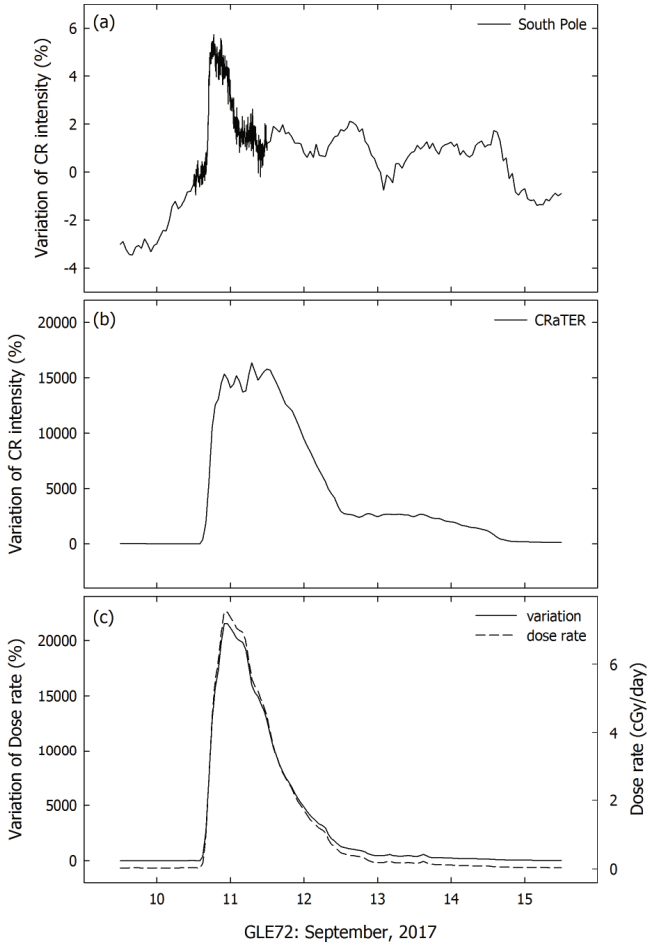

Fig. 4. Hourly profiles of CRE recorded on 10 September 2017 (C96) associated with GLE72 terrestrial on Earth. From top to bottom, each panel represents the variations in CR intensity (a) at the terrestrial South Pole neutron monitor and (b) at the lunar surface by CRaTER and (c) the variation in dose rate by micro-dosimeter in CRaTER in the lunar radiation environment.

summations of counts by single counters, good counts include all count events exclusive of duplicated signals at each single counter. Therefore, good counts can represent the proton flux in the energy range above 12.7 MeV. We considered good counts in this study to be those with CR intensity above 12.7 MeV according to CRaTER.

The 5 min data of CR intensity are typically used to create the GLE profile. However, because a CRE profile of 5 min shows noisy variation with large fluctuations, it is difficult to determine the exact onset of CRE. Figure 2 presents the hourly counts (thin gray line), 3 hr weighted smoothed data (thick black line), and 110 min data (red line) for day of year (DOY) 168-162 in 2010 (a) and DOY 160 in 2010 (b). Because the orbital period of the LRO is 110 min, hourly counts show the oscillation with alternating highs and lows (Fig. 2). As shown in Fig. 2(b), 110 min data cover one day in only 13.09 intervals. Therefore, the profile of CR intensity in 110 min data is shifted from original data, as shown by the red line in the figure. Even though they are averaged, the 3 hr smoothed (running averaged) data have 24 intervals for each day. Because they have also been computed by weighting (0.25/0.5/0.25), the value of each hour can maintain the original trend of variation. The 3 hr smoothed data show a variation trend in counts because the oscillation from the orbital period is deleted. Thus, we smoothed the hourly count and dose rate data by using 3 hr weighting to determine the trend of increase.

In general, GLEs are associated with solar flare-accelerated particles that are classified by SPE using the proton flux measured by GOES series satellites. An SPE has a flux greater than 10 MeV protons and greater than 10 particles $cm^{-2}sec^{-1}sr^{-1}$ (particle flux units: pfu), as defined by NOAA SESC. As previously mentioned,

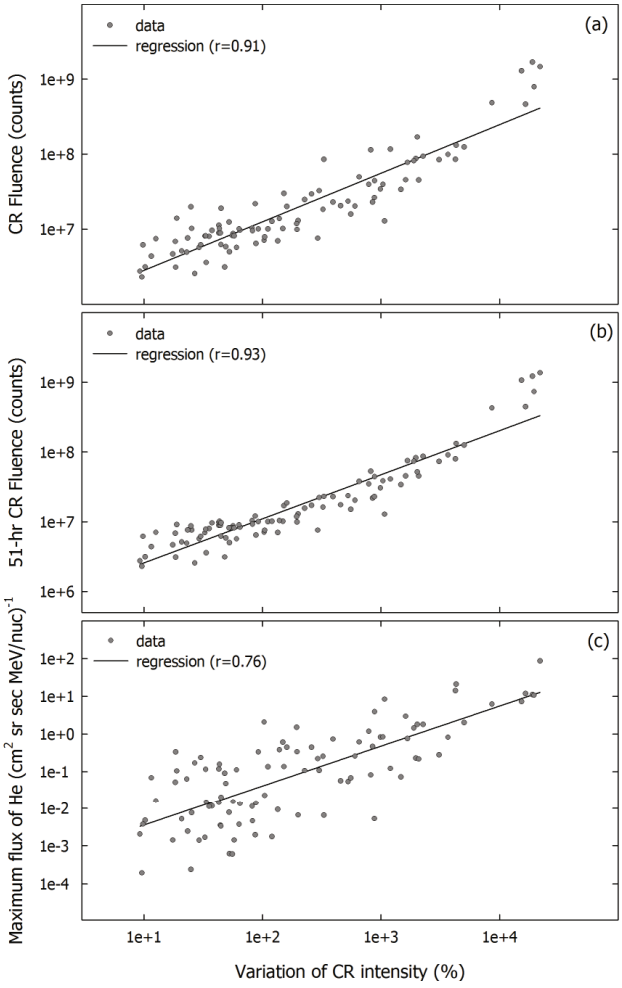

Fig. 5. Comparison of variation in CR intensity and (a) CR fluence, (b) 51 hr CR fluence, and (c) maximum flux of He (3.43–4.74 MeV/n) observed by ACE/SIS for 96 CREs.

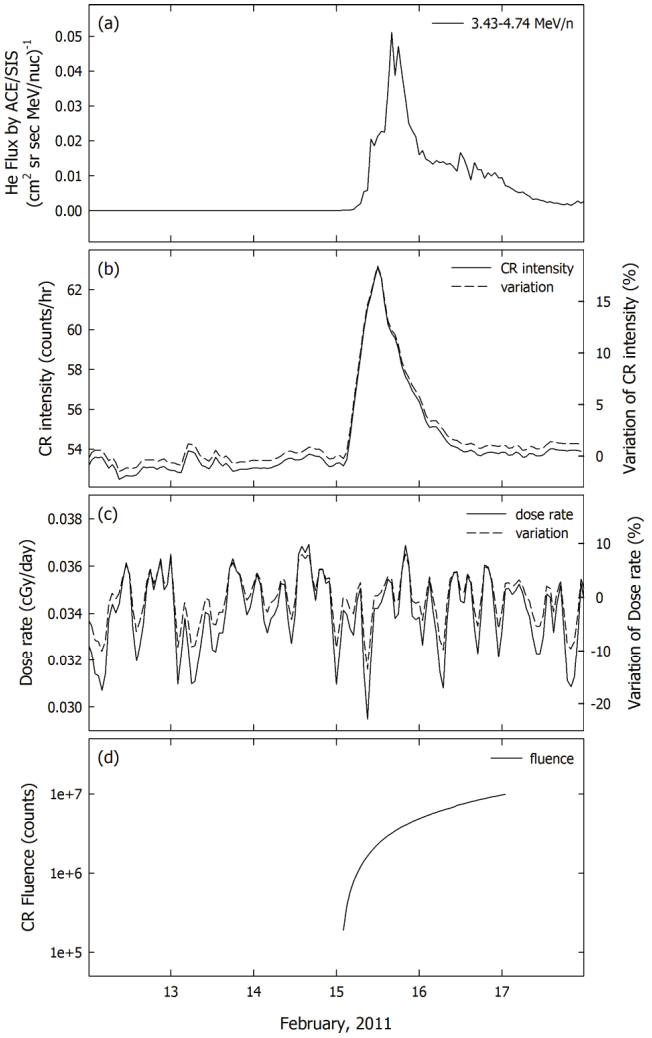

Fig. 6. Time profiles of CRE without associated SPEs recorded on 15 February 2011 (C05): (a) He flux in the energy range of 3.43–4.74 MeV/n by ACE/SIS, (b) CR intensity and variation in CR intensity (%), (c) dose rate and variation in dose rate (%), and (d) CR fluence for the entire event period.

CRaTER can detect protons above 12.7 MeV; therefore, it is useful to monitor SPEs as well as GCRs [2].

We drew the time profiles of CR intensity and dose rates observed by CRaTER. Then, we selected the associated solar events from the solar flare and SPE data of NOAA SESC (http://umbra.nascom.nasa.gov/SEP). In addition, we compared the hourly CR data observed by SIS onboard ACE (http://www.srl.caltech.edu/ACE/ASC/level2/lvl2DATA_SIS.html). ACE/SIS provides solar energetic particle measurements for species of Z = 0–28 in the range of 5–150 MeV/nuc. Among fourteen species and eight energy ranges, we selected He in the lowest energy range, which has a high abundance for verifying the reliable value. The ACE/SIS team provides the energy ranges for each species. That of the zero-band for He is 3.43 MeV/n (minimum) to 4.74 MeV/n (maximum), and the mean energy is calculated by the square root of the minimum × the maximum. Thus, the zero-band has a mean of 4.03 MeV/n, which is energy per nucleon. In the zero-band, He itself has a mean energy of 16.12 MeV. Moreover, it is four times heavier than a proton, and its velocity is half the velocity of a proton at the same solar event. The abundance ratio of He in the zero-band is reliable and larger than that in any other band. Therefore, it may be proper to compare the CR intensity by using CRaTER with flux of He in the zero-band by using ACE/SIS data.

We investigated the CR intensity variations in the lunar space environment in a manner similar to that for terrestrial GLEs. We examined the increasing events having variation greater than about 10% of each GCR background. The background is defined as the average of two days prior to CRE onset. When the CREs occurred successively and their backgrounds were disturbed, we selected the quiet background before the first CRE out of the successive event occurrence. Thus, we defined the CR intensity variation (%) of CREs on the lunar surface.

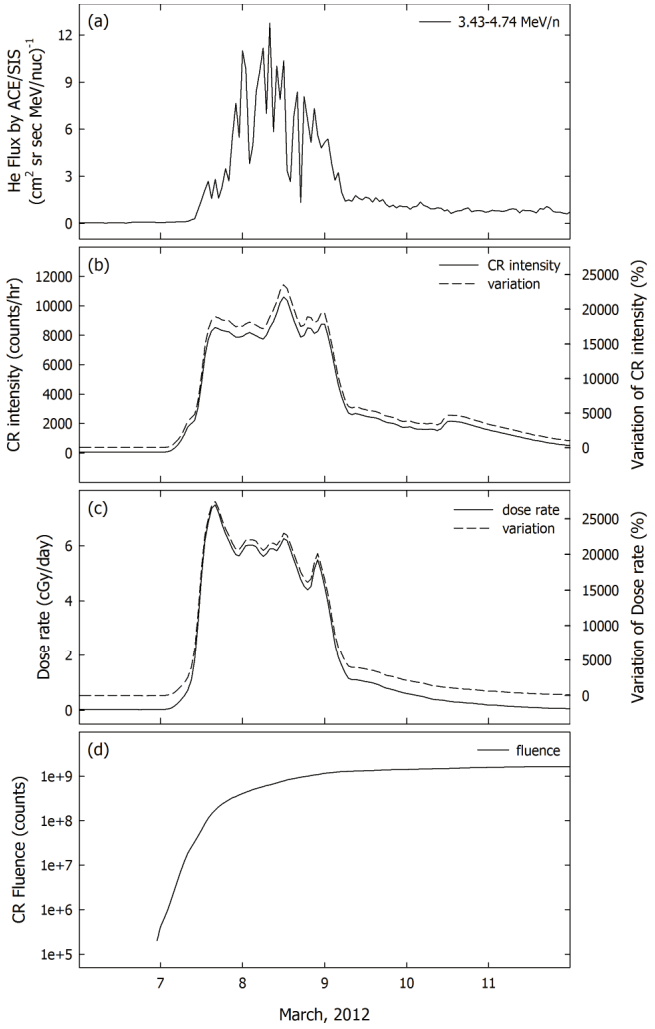

Fig. 7. Time profiles of CRE with associated SPEs recorded on 7 March 2012 (C24): (a) He flux in the energy range of 3.43–4.74 MeV/n by ACE/SIS, (b) CR intensity and variation in CR intensity (%), (c) dose rate and variation in dose rate (%), and (d) CR fluence for the entire event period.

We identified 96 CREs from June 2009 to December 2017. To examine their origins and characteristics, we compared the time variation profile of the CRaTER counts with those of ACE/SIS and SPE data. To verify the CREs identified by variation in the CRaTER counts, we also checked the time profile of micro-dosimeter measurement for coincidence; this instrument is housed within the CRaTER instrument. J. E. Mazur *et al.* compared the relative changes in the dosimeter rate and the GCR proton measurement > 10 MeV by using ACE/SIS data; good agreement was reported. Even though the micro-dosimeter was not designed for scientific purposes, it effectively monitors even relatively small changes in the GCR environment [3]. This result suggests that the micro-dosimeter can explain the dose rate in energy of above 10 MeV. Thus, we consider that the realistic cutoff energy of the dosimeter is about 10 MeV, which is similar to the cutoff of CR intensity by CRaTER.

III. RESULTS

1. Identification of CREs in the Lunar Space Environment

Table 1 lists the 96 CREs in the lunar space environment between June 2009 and December 2017. The leftmost column contains the event number; year; date of background; averaged count during the background period as the baseline; onset time and maximum time; variation in CR intensity at the maximum time; CR fluence (counts) during the event period; CR fluence (counts) for 51 hr, which is the median value of duration; onset time of associated SPE and its proton flux; date of lunar calendar; and position. The background date indicates the start date of the background period, 49 hr. To calculate the fluence of CRE, we selected the time at which the count recovered the level before CRE for the end time of the event. Additionally, the position indicates whether the point is located in or out of the Earth's magnetosphere in a lunar orbit when each CRE occurred. The SPE data (https://umbra.nascom.nasa.gov/SEP/) were provided by NOAA SESC.

Figure 3 shows the hourly profiles of CRE on 17 May 2012 (C26) associated with terrestrial GLE71. The top to bottom panels each represent the variations in CR intensity at the terrestrial South Pole neutron monitor (a) and at the lunar surface by CRaTER (b) in addition to the variation of dose rate by micro-dosimeter in CRaTER (c) in the lunar space environment. Three profiles approximately coincide in their onsets and resemble one another. They show a sharp onset followed by a decline as a sharp increase in the main phase and a gradual recovery phase. We can confirm the similarity of the time profiles of CR intensity and dose rate. The difference is that the CREs lasted longer than the GLEs. Because of the SPE time profiles with energy, higher-energy protons fell off faster than lower-energy ones, and most of protons measured by CRaTER were nearly 100 times less energetic than those that caused GLEs.

Figure 4 shows another example of a CRE on 10 September 2017 (C96) associated with terrestrial GLE72. The trends shown in this figure are the same as those shown in Fig. 3. GLE71 had a larger percentage increase than GLE72, although C26 had a smaller variation of CR intensity than C96.

Figure 5 shows the relationship between the variation of CR intensity and CR fluence (a), 51 hr CR fluence (b), and maximum flux of He in the energy range of 3.43–4.74 MeV/n observed by ACE/SIS (c) for all CREs. Circles indicate the CRE values, and solid lines indicate their regression lines. Because the length of an event can affect the fluence for the entire event period, we also defined 51 hr CR fluence. As shown in Table 1, 51 hr

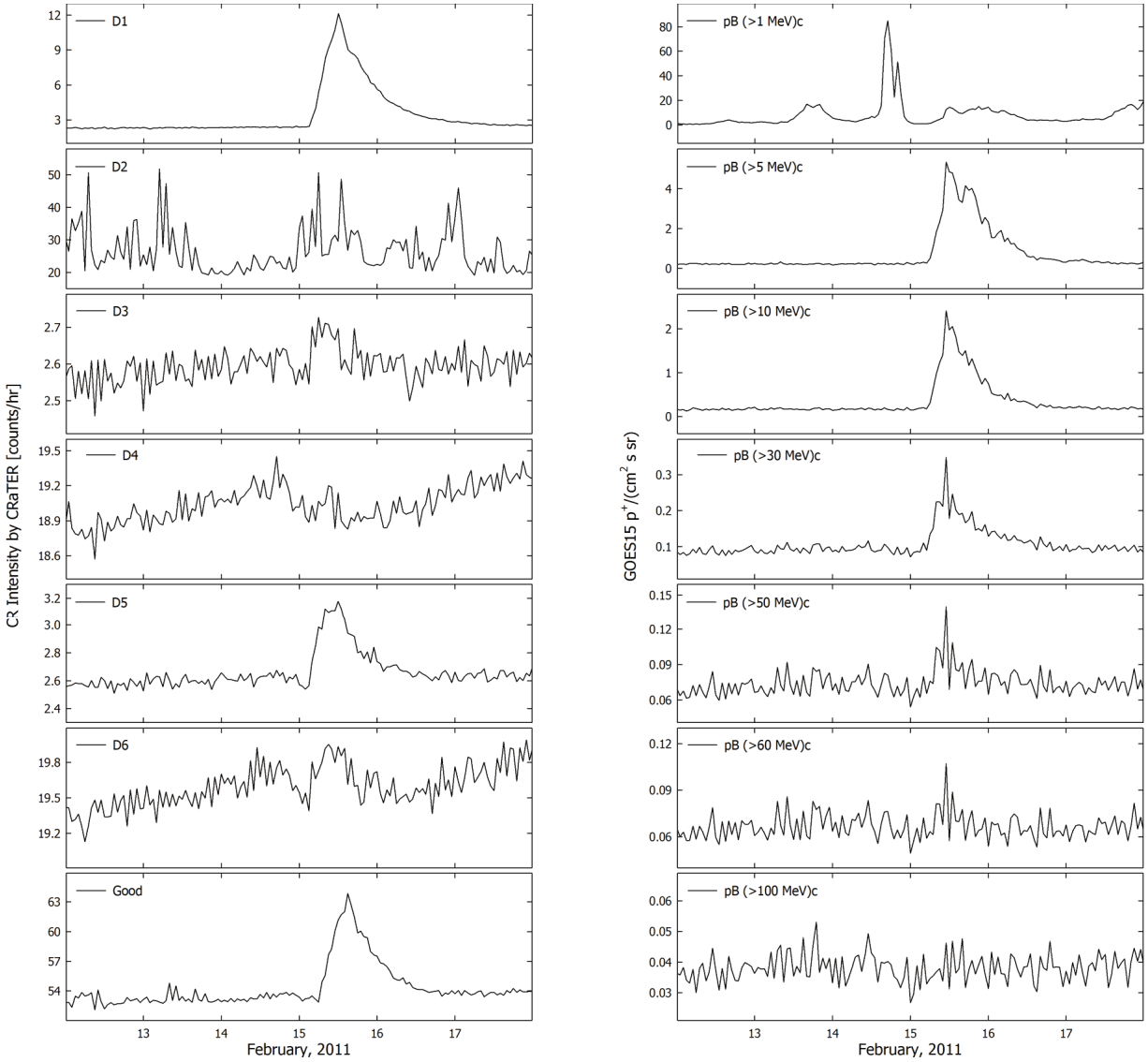

Fig. 8. Time profiles of CR intensity in single six channels (D1-D6) and good counts (as the total counts) by CRaTER (left) and time profiles of corrected integrated proton flux in the seven channels by the B detector of GOES15 (right) for CREs without associated SPEs on 15 February 2011 (C05).

is a representative value as the median duration. To calculate the fluence of SPE, S. Y. Oh *et al.* used a half-day interval beginning at the peak as the event length of an SPE [12]. A 51 hr duration of CRE is longer than the length of the SPE, which is associated with the CRE. The variation in CR intensity as the magnitude of CRE has a good relationship with CR fluence, 51 hr CR fluence, and maximum flux of He. It has a lower correlation coefficient with the maximum flux of He than with 51 hr CR fluence because the abundance of He at the Sun is one-third in mass ratio and one-tenth in number compared with the proton at the photosphere. Additionally, because He is heavier than the proton, the distribution of its energy is different at the same solar event. This comparison is suitable for examining the origins of CREs with the assumption that an increase in He flux is associated with a solar event regardless of whether it is accompanied by an SPE.

2. Classification of CREs Based on the Association of SPE

Figure 6 shows the CRE time profiles with no associated SPE on 15 February 2011 (C05). From top to bottom, the panels in the figure display He flux in energy range of 3.43–4.74 MeV/n by ACE/SIS (a), the CR intensity and variation of CR intensity (%) by CRaTER (b), the dose rate and variation of dose rate (%) by microdosimeter (c), and the CR fluence by CRaTER for the

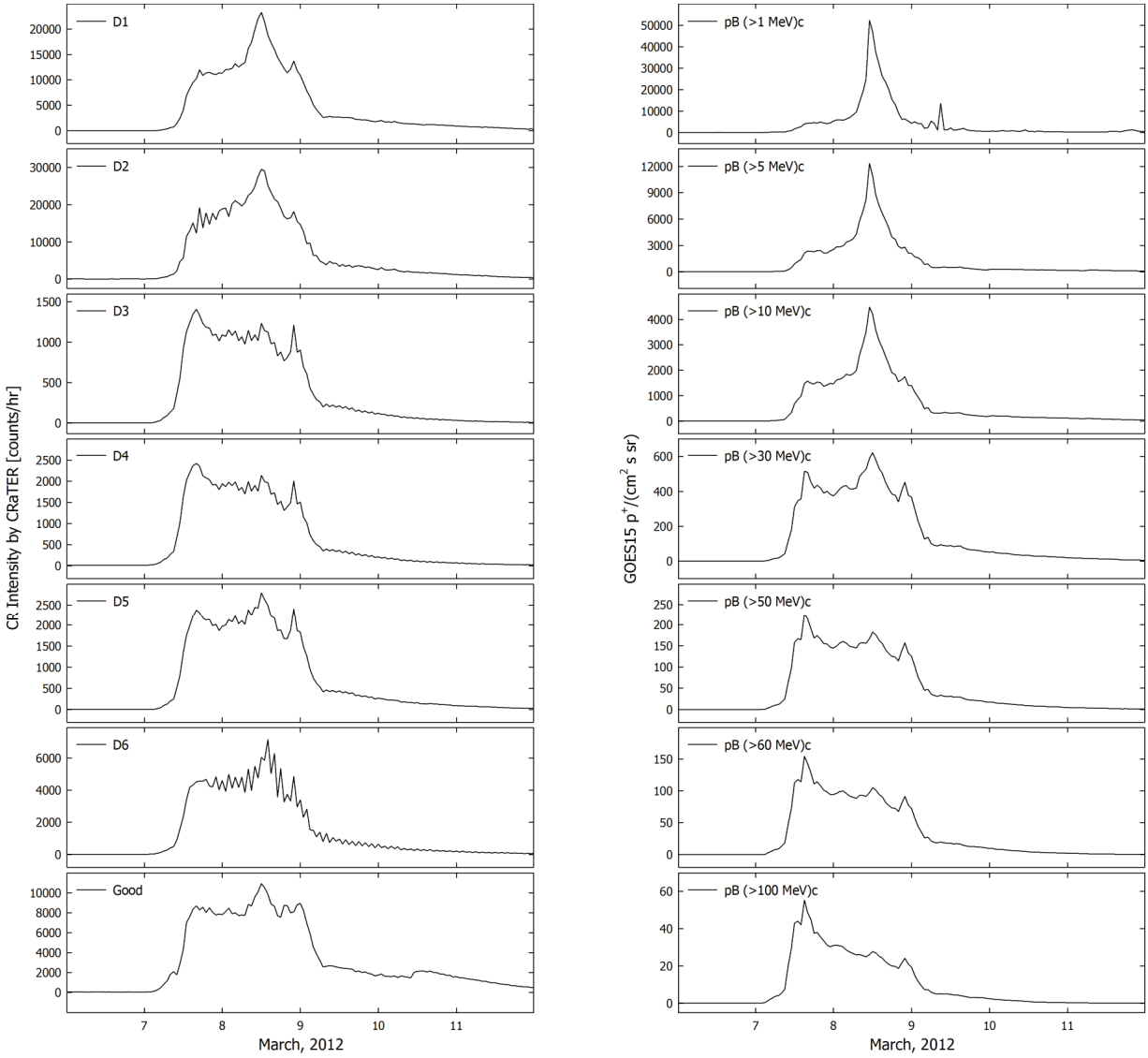

Fig. 9. Time profiles of CR intensity in single six channels (D1-D6) and good counts (as the total counts) by CRaTER (left) and time profiles of corrected integrated proton flux in the seven channels by the B detector of GOES15 (right) for CREs with associated SPEs on 7 March 2012 (C24).

entire event period (d). Figure 7 shows the CRE time profiles with associated SPEs on 7 March 2012 (C24). The display of Fig. 7 is the same as that in Fig. 6.

C05 in Fig. 6 shows an approximate 18% increase in CR intensity and a significant but weak increase in He flux. However, the dose rate shows no significant increase during the CRE period. This CRE has a low CR fluence and a short event length. C24 in Fig. 7 shows large increase, with an approximate 26,000% increase in CR intensity and 27,000% increase in dose rate. The He flux by ACE/SIS also shows a large increase during the CRE. This CRE maintained its increased value for about two days. Moreover, it has a large CR fluence. The variation in CR intensity for C24 during the event period is approximately 1,300 times greater than that of C05.

Figure 8 shows the time profiles of CR intensity and proton flux for C05. The left panel shows the time profiles of CR intensity in single six channels (D1-D6) and good counts by CRaTER, and the right panel shows the time profiles of corrected integrated proton flux in seven channels by detector B of GOES15. Figure 9 shows the time profiles of CR intensity and proton flux for C24. The display of Fig. 9 is the same as that in Fig. 8.

In the single channel count, only D1 and D5 showed a significant increase for C05 in Fig. 8. The count increase of D1 indicates that the space (zenith) is the direction of the entering protons. For incident CR particles from the zenith, the proton threshold energies were 12.7 and 114.5 MeV for the first pair of thin (D1) and thick (D2) silicon detectors and the pair (D1 and D6), respectively. This indicates that the proton that passes the first pair of silicon detectors and reaches the last silicon detec-

Table 2. Averaged values for two classes of CREs based on the association of SPEs.

	Number of events	Variation (%)	CR fluence (counts)	51 hr CR fluence (counts)	Duration (hr)	Maximum flux of He $(cm^2$ sr sec MeV/n$)^{-1}$
All	96	1,598.05	9.00E+07	7.50E+07	62.71	2.16E+00
		(127.26)	(1.25E+07)	(1.01E+07)	(51)	(1.06E-01)
w/ SPE	43	3,443.21	1.87E+08	1.57E+08	77.40	4.75E+00
		(988.26)	(4.40E+07)	(3.84E+07)	(66)	(7.56E-01)
wo/ SPE	53	101.03	1.11E+07	8.70E+06	50.79	6.35E-02
		(44.19)	(8.11E+06)	(7.74E+06)	(45)	(1.33E-02)
Student's t-Test	t	4.18	3.29	3.33	3.51	2.50
	P-value	0.0001	0.0014	0.0012	0.0007	0.014

The values in brackets indicate the median value of each item.

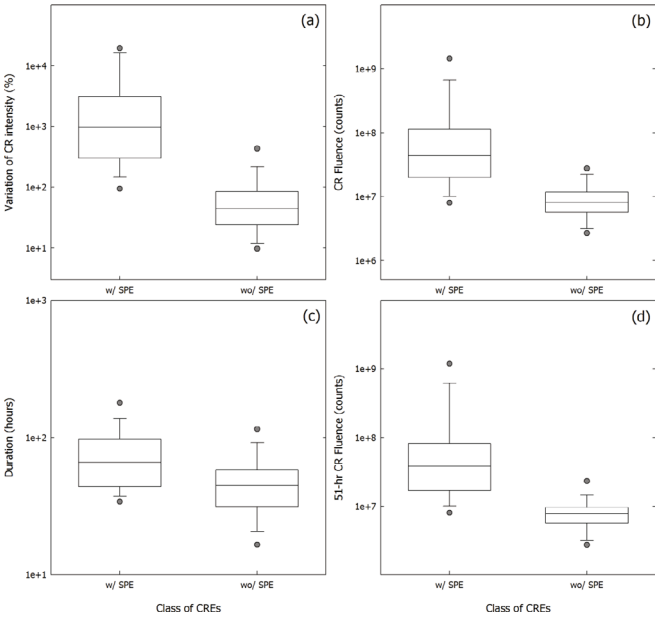

Fig. 10. Ranges of physical properties for CREs with and without associated SPE: (a) variations in CR intensity, (b) CR fluence, (c) duration, and (d) 51 hr CR fluence.

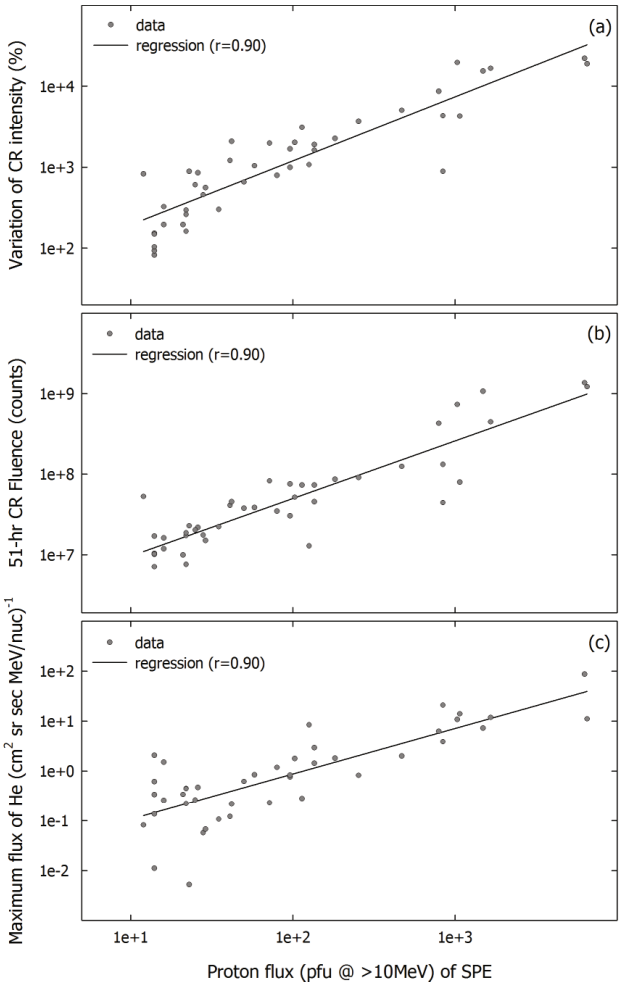

Fig. 11. Relationship between proton flux of SPEs and variations in (a) CR intensity, (b) 51 hr CR fluence, and (c) maximum flux of He by ACE/SIS for CREs with associated SPEs.

tor (D6) can be detected in the energy range of at least 12.7–114.5 MeV. In the proton flux of GOES15 channels, most of solar protons are distributed in the range below 10 MeV in this CRE. These small increases indicate that the lunar space environment responds to small solar variations.

Unlike C05 without associated SPEs, all single channels of CRaTER show a large increase for C24 in Fig. 9, and all integrated proton channels of GOES15 show a significant increase. It is important to note that G24 is closely related to a high proton flux of $>\sim 10$ MeV.

CREs with associated SPEs showed a CR intensity variation of more than 100%. The magnitude of CREs with associated SPEs was larger than that without associated SPE, as confirmed in Table 2. The table displays the averaged values in variation of CR intensity, CR fluence, 51 hr CR fluence, duration, and maximum flux of He by ACE/SIS for CREs with and without associated SPE. The values in brackets indicate the median

Table 3. Correlation coefficients between variations in CR intensity and other physical properties.

	CR fluence (count)	51 hr CR fluence (count)	Maximum flux of He (cm^2 sr sec MeV/n)$^{-1}$
w/ SPE	0.92	0.94	0.65
wo/ SPE	0.72	0.81	0.26
All	0.91	0.93	0.76

value of each characteristic. Of the 96 CREs, 43 events were associated with SPEs. The values of their physical characteristics are 10 times larger than those without associated SPEs. These differences between CREs with and without associated SPE were statistically examined by Student's t-Test. At a significance level of 0.05, each characteristic except for the maximum flux of He can reject the null hypothesis that there is no difference in averages between the two classes based on the association of SPEs. This result is presented in the last row of Table 2.

Figure 10 shows a box plot of the ranges for CREs with and without associated SPE. The boundary of the box closest to zero indicates the 25th percentile, a line within the box marks the median, and the boundary of the box farthest from zero indicates the 75th percentile. Two circles above and below the box indicate the 90th and 10th percentiles. As shown in Table 2, Fig. 10 also shows the difference in the ranges of the physical characteristics, except for duration, between CREs with and without associated SPE.

Figure 11 shows the relationship between the proton flux of SPE and the physical characteristics of CREs with associated SPE. The circles indicate values of CREs with associated SPEs, and the solid lines indicate their regression lines. The proton flux of SPEs shows good correlation with the variation in CR intensity (a), 51 hr CR fluence (b), and maximum flux of He by ACE/SIS (c).

Table 3 shows the correlation coefficients between the variation of CR intensity and other physical characteristics. All CREs have good correlation, although CREs with associated SPEs have better correlation than those without. This relationship is also shown in Fig. 12.

Figure 12 indicates the relationship of the two classes based on the association of SPEs between the variation of CR intensity and CR fluence (a), 51 hr fluence (b), and maximum flux of He by ACE/SIS (c). The circles and down triangles represent CREs with and without associated SPE, respectively. The solid and dashed lines indicate their regression lines. CREs with associated SPEs show better correlation than those without.

As previously mentioned, SPEs are the main source of CREs in the lunar space environment. Even though CREs occur without associated SPEs, they are also related to the solar activity of solar ejection. Even a small increase in GOES15 proton channels and He flux by

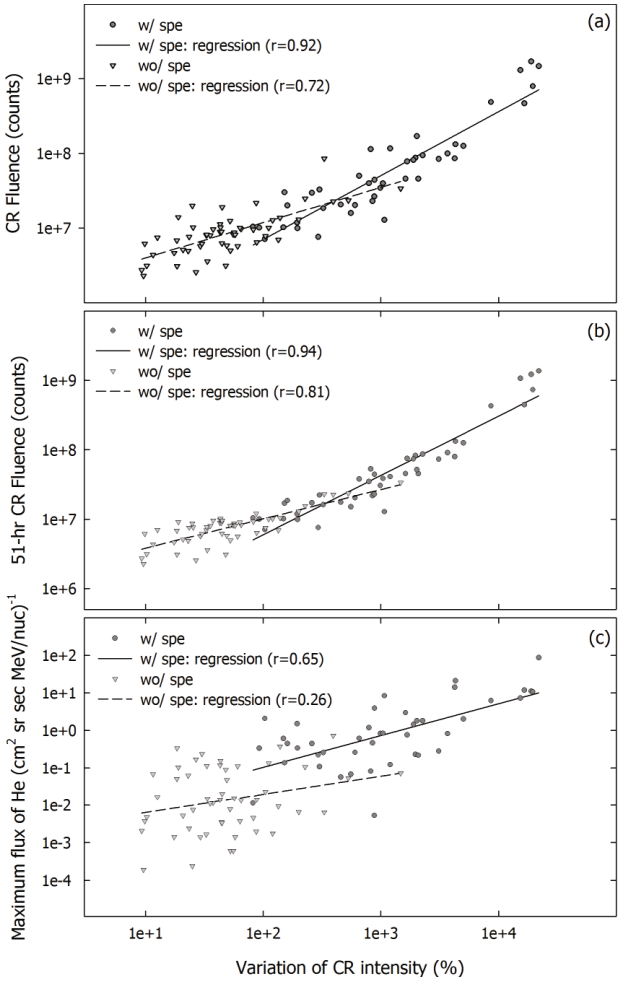

Fig. 12. Relationship of two classes based on the association of SPEs between variations in CR intensity and (a) CR fluence, (b) 51 hr CR fluence, and (c) maximum flux of He by ACE/SIS. The circles and triangles represent CREs with and without associated SPEs, respectively. The solid and dashed lines indicate their regression lines.

ACE/SIS indicates that some particles are ejected from the Sun. In fact, all CREs are associated with solar eruptions such as solar flares. The solar flares and CREs exhibit a one-to-one correspondence (not shown in Table 1). Therefore, the lunar space environment responds to each solar ejection because of the very weak magnetic field and almost vacuum atmosphere.

IV. DISCUSSION AND CONCLUSTION

We identified 96 CREs in the lunar space environment by using CR intensity measured by CRaTER between June 2009 and December 2017. To ensure reliability, we also compared the dose rate by using a microdosimeter within CRaTER, CR data by ACE/SIS, and proton flux by GOES15. These events are similar to the

GLEs recorded in the Earth's ground neutron monitors, showing increases with a sharp increasing profile. However, the CREs showed different characteristics from the terrestrial GLEs with much longer and more frequent occurrences than terrestrial GLEs. For example, 96 CREs were identified with an average duration of 51 hr during the analysis period; in contrast, only two terrestrial GLEs occurred (GLE71, GLE72) and had short durations of < 12 hr.

Of the 96 CREs, 43 events are associated with SPE. The values of their physical characteristics were statistically larger than those without associated SPEs, as shown in Table 2. However, solar ejections are considered to be the origin of CREs without associated SPE, according to the analysis of CR data by ACE/SIS. All CREs are associated with an increase in He flux by ACE/SIS. Despite the small increase in He flux and GOES15 proton channels, some materials were ejected from the Sun, which means that all CREs are associated with solar eruptions such as solar flares. We can make a one-to-one correspondence between solar flares and CREs. Therefore, the lunar space environment responds to each solar ejection because of the very weak magnetic field and almost vacuum atmosphere. As [16] reported, the space environment must be carefully considered in planning for future space missions. Additionally, an increase in He flux observed by ACE/SIS can be a good index for monitoring the eruption of energetic particles from the Sun by supplementation of SPEs.

ACKNOWLEDGMENTS

This work was supported by basic research funding from the Korea Astronomy and Space Science Institute. This research was also supported by the Basic Science Research Program through the National Research Foundation of Korea (NRF), funded by the Ministry of Education (NRF-2018R1D1A1B07046522). Yu Yi was supported by the Basic Science Research Program through the National Research Foundation of Korea (NRF), funded by the Ministry of Education (NRF-2016R1D1A3B03933339). The authors greatly appreciate support from the LRO/CRaTER project under contract NASA NNG05EB92C. The authors also are grateful to the ACE/SIS team, the NOAA Space Environment Services Center, the directors of Bartol Research Institute, and the GOES Space Environment Monitor team.

REFERENCES

[1] C. R. Tooley, M. B. Houghton, R. S. Saylor Jr., C. Peddie, D. F. Everett *et al.*, Space Sci. Rev. **150**, 23 (2010).
[2] H. E. Spence, A. W. Case, M. J. Golightly, T. Heine, B. A. Larsenet *et al.*, Space Sci. Rev. **150**, 243 (2010).
[3] J. E. Mazur, W. R. Crain, M. D. Looper, D. J. Mabry, J. B. Blake *et al.*, Space Weather **9**, S07002 (2011).
[4] S. Oh and J. Kang, J. Astron. Space Sci. **30**, 175, (2013).
[5] J. Jung J, S. Oh, Y. Yi, P. Evenson, R. Pyle *et al.*, J. Astron. Space Sci. **33**, 345 (2016).
[6] S. Oh and Y. Yi, J. Astron. Space Sci. **23**, 117 (2006).
[7] S. E. Forbush, Phys. Rev. **51**, 1108 (1937).
[8] S. Oh, J. Astron. Space Sci. **25**, 149 (2008).
[9] S. Lee, S. Oh, Y. Yi, P. Evenson, G. Jee *et al.*, J. Astron. Space Sci. **32**, 33 (2015).
[10] A. Belov, E. Eroshenko, H. Mavromichalaki, C. Plainaki and V. Yanke, Adv. Space Res. **35**, 697 (2005).
[11] S. E. Forbush, Phys. Rev. **70**, 771 (1946).
[12] S. Y. Oh, Y. Yi, J. W. Bieber, P. Evenson and Y. K. Kim, J. Geophys. Res.: Space Phys. **115**, A09105 (2010).
[13] S. Y. Oh, J. W. Bieber, P. Evenson, J. Clem, R. Pyle *et al.*, Space Weather **10**, S05004 (2012).
[14] N. A. Schwadron, T. Baker, J. B. Blake, A. W. Case, J. F. Cooper *et al.*, J. Geophys. Res.: Space Phys. **117**, E00H13 (2012).
[15] N. A. Schwadron, J. B. Blake, A. W. Case, C. J. Joyce, J. Kasper *et al.*, Space Weather **12**, 622 (2014).
[16] N. A. Schwadron, F. Rahmanifard, J. Wilson, A. P. Jordan, H. E. Spence *et al.*, Space Weather **16**, 289 (2018).